frontiers | Frontiers in Chemistry

TYPE Original Research
PUBLISHED 13 December 2022
DOI 10.3389/fchem.2022.1040435

OPEN ACCESS

EDITED BY
Hassan Ait Ahsaine,
Mohammed V University, Morocco

REVIEWED BY
Mohamed Zbair,
UMR7361 Institut de Sciences des Matériaux de Mulhouse, France
Mohamed El Ouardi,
Mohammed V University, Morocco

*CORRESPONDENCE
Yun Zhang,
zhangyun1977@syau.edu.cn

†PRESENT ADDRESS
Xin Liu,
Symgreen Environmental Technology Co., Ltd., Beijing, China

SPECIALTY SECTION
This article was submitted to Inorganic Chemistry, a section of the journal Frontiers in Chemistry

RECEIVED 12 September 2022
ACCEPTED 24 October 2022
PUBLISHED 13 December 2022

CITATION
Sun X, Chen M, Lei J, Liu X, Ke X, Liu W, Wang J, Gao X, Liu X and Zhang Y (2022), How β-cyclodextrin- loaded mesoporous SiO_2 nanospheres ensure efficient adsorption of rifampicin. *Front. Chem.* 10:1040435. doi: 10.3389/fchem.2022.1040435

How β-cyclodextrin- loaded mesoporous SiO_2 nanospheres ensure efficient adsorption of rifampicin

Xun Sun[1,2], Mingming Chen[2], Jiayu Lei[2], Xinran Liu[2], Xin Ke[2], Wengang Liu[3], Jingkuan Wang[1], Xiaodan Gao[1], Xin Liu[2†] and Yun Zhang[1*]

[1]Northeast Key Laboratory of Arable Land Conservation and Improvement, Ministry of Agriculture, College of Land and Environment, Shenyang Agricultural University, Shenyang, China, [2]Liaoning Key Laboratory of Clean Energy and College of Energy and Environmental, Shenyang Aerospace University, Shenyang, China, [3]School of Resources and Civil Engineering, Northeastern University, Shenyang, China

In this study, β-CD@mesoporous SiO_2 nanospheres (β-CD@mSi) were prepared by loading β-cyclodextrin (β-CD) onto mesoporous silica nanospheres through an *in situ* synthesis. This not only solved the defect of β-CD being easily soluble in water, but also changed the physical structure of the mesoporous silica nanospheres. FTIR and XPS results showed that β-CD was successfully loaded onto mesoporous silica nanospheres (mSi), while enhancing the adsorption effect. β-CD@mSi with a monomer diameter of about 150 nm were prepared. At a temperature of 298k, the removal efficiency of a 100 mg/L solution of rifampicin can reach 90% in 4 h and the adsorption capacity was 275.42 mg g^{-1} at high concentration. Through the calculation and analysis of adsorption kinetics, adsorption isotherms and adsorption thermodynamics based on the experimental data, the reaction is a spontaneous endothermic reaction dominated by chemical adsorption. The electron transfer pathway, structure–activity relationship and energy between β-CD@mSi and rifampicin were investigated by quantum chemical calculations. The accuracy of the characterization test results to judge the adsorption mechanism was verified, to show the process of rifampicin removal by β-CD@mSi more clearly and convincingly. The simulation results show that π–π interaction plays a major interaction in the reaction process, followed by intermolecular hydrogen bonding and electrostatic interactions.

KEYWORDS

β -cyclodextrin, mesoporous silica nanospheres, rifampicin, adsorption, simulated calculation

1 Introduction

Rifampicin (RIF) is a major and effective drug for the treatment of tuberculosis (Damasceno et al., 2020). The overuse and misuse of antibiotics has led to increased bacterial resistance, posing significant risks to the water resources and human health (Rodriguez-Mozaz et al., 2015). Therefore, it is necessary to find a feasible and effective technology to eliminate RIF in the water environment.

So far, many methods, such as biodegradation (Xiong et al., 2016), membrane filtration (Wang et al., 2021), photocatalytic degradation (Wang et al., 2018), AOPs (Kanakaraju et al., 2019), and adsorption (Zhao et al., 2019) have been applied to remove antibiotics from wastewater, the adsorption is considered to be an effective method among the above methods (Wei et al., 2019). Compared to other processes, adsorption has the advantages of high efficiency, low cost, regenerability and ease of operation (Mallik et al., 2022).

Traditional inorganic adsorbents are widely used in environmental remediation. Among these inorganic materials, mesoporous silica nanoparticles (MSNs) are more suitable for practical applications due to their adjustable structure (Yin et al., 2019). Grafting organics with special properties onto silicon-based materials can be considered to form new composite structure to enhance their ability to remove specific pollutants (Stephanie et al., 2012; Zhang et al., 2019). β-CD is a barrel oligosaccharides (Tian et al., 2020). Its cavity is hydrophobic inside and hydrophilic outside, due to the activity of edge hydroxyl groups, can form inclusion complexes with pollutants (Sikder et al., 2018). Kuang, silanized Fe304@SiO2 A novel magnetic surface molecularly imprinted polymer (HC/SMIPs) was prepared for the specific extraction of 4-hydroxycoumarin. The maximum adsorption capacity of HC/SMIPs could reach to 22.78 mg/g (Kuang et al., 2022). Marrane describe a novel approach for *in situ* synthesis of cellulose microfibrils-*grafted*-hydroxyapatite (CMFs-*g*-HAP_N (8%)) as an adsorbent using phosphate rock and date palm petiole wood as alternative and natural Moroccan resources. The maximum adsorption capacities of the CMFs-g-HAPN (8%) adsorbent toward Pb(II) and Cu(II) are 143.80 and 83.05 mg/g (Marrane et al., 2022). Since rifampicin has a similar functional group structure to the above pollutants, therefore, β-CD loaded mesoporous silica nanospheres can be used to try to remove rifampicin.

At present, there are few research on the removal of rifampicin from water environment, mainly focusing on adsorption at low concentration. The explanation of rifampicin adsorption mechanism is not sufficient. In order to solve these problems, in this study, with 3-methacryloxypropyltrimethoxysilane (KH570) as cross-linker, β-CD was loaded onto mesoporous silica nanospheres to remove RIF from aqueous solution (Figure 1). We conducted batch experiments with different factors to explore the optimal reaction conditions of RIF, and verified its adsorption capacity under high concentration. Due to the limitations of current characterization test techniques in describing electron behavior, it is difficult for these methods to provide absolutely correct results. Quantum chemical calculations can provide detailed structural and energy information (Ma et al., 2016; Liu et al., 2019), and this is necessary to study the reaction process. In order to better explain the adsorption mechanism, the density functional theory (DFT) was used as the calculation basis, the possible activation sites of β-CD and RIF were predicted by computer simulation, the electron migration path and the intermolecular interaction were verified (De et al., 2016; Khnifira et al., 2020; Mao et al., 2021). The priority of chemical reactions in the adsorption process is further elaborated, and the adsorption process of antibiotics is better explained from the electronic level.

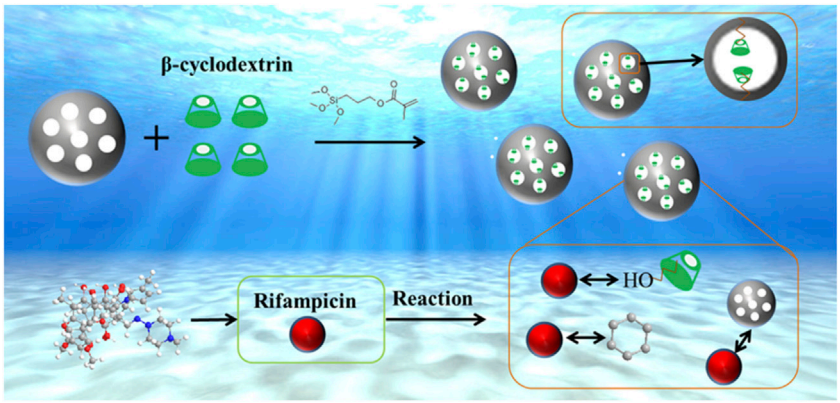

FIGURE 1
The adsorption process of RIF.

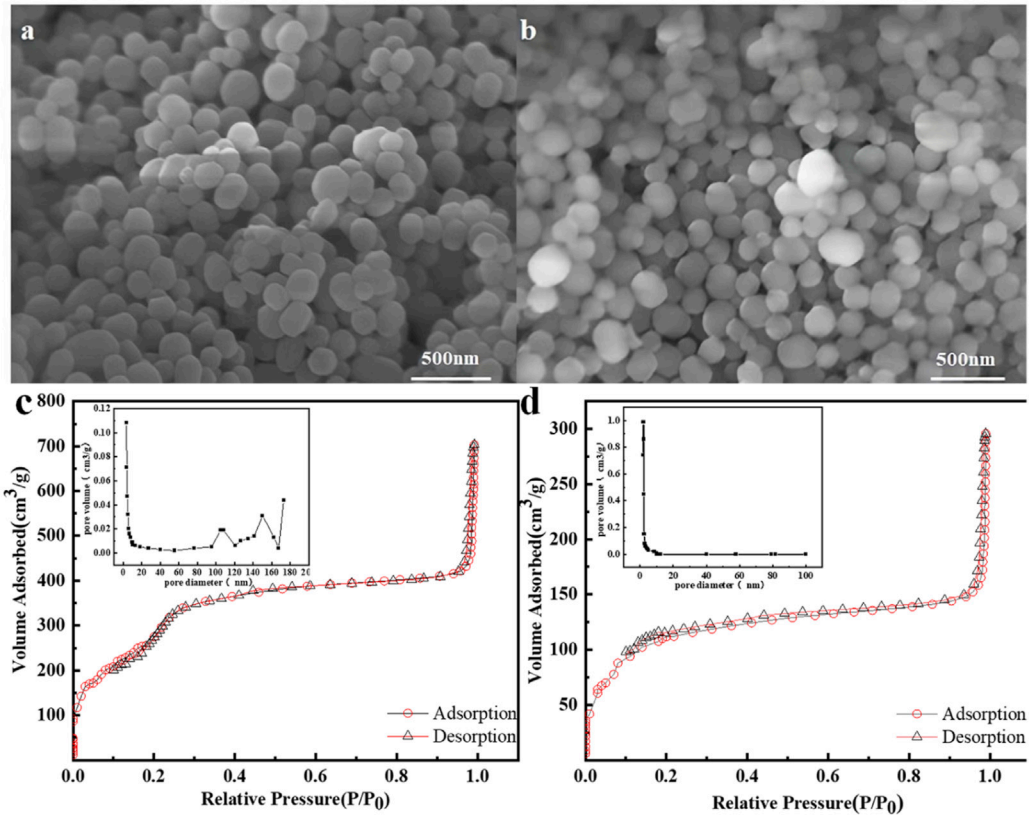

FIGURE 2
(A) SEM image of mSi; **(B)** SEM image of β-CD@mSi; **(C)** Nitrogen adsorption-desorption isotherm for mSi; **(D)** Nitrogen adsorption-desorption isotherm for β-CD@mSi.

2 Reagents and methods

2.1 Chemicals

Rifampicin was supplied by Shenyang Pharmaceutical Company. β-CD ($C_{42}H_{70}O_{35}$, 98%) and cetyltrimethylammonium bromide (CTAB; $C_{19}H_{42}BrN$, 99%) were purchased from Shanghai Aladdin company. Tetraethyl orthosilicate (TEOS) was purchased from Tianjin chemical reagent factory. In this study, all chemical reagents were of analytical grade, and all solutions are prepared with pure water.

2.2 Composite material preparation

2.2.1 Preparation of mesoporous SiO_2 nanospheres

The whole experiment was carried out under water bath conditions (80°C). About 1 g CTAB was added to 500 ml deionized water, which was then placed in a magnetic stirrer and stirred until the solution is clear and transparent. The speed was increased and 3.5 ml of 2 mol/L NaOH solution was added, and then 5 ml of TEOS was added slowly. Stirring was continued for 2 h, and the extracted white solids were washed with deionized water for three times. After freeze-drying, it was put into a muffle furnace and calcined at 550°C in an air atmosphere for 4 h (heating rate 10°C/min) to obtain mesoporous SiO_2 nanospheres.

2.2.2 Preparation of β-CD@mSi

Mesoporous silica powder suspension (pH = 4) was prepared and placed in a magnetic stirrer for stirring, while adding 1 ml KH570 and 20 ml β-CD solution (pH = 4). It was stirred and allowed to react for 6 h to obtain β-CD@SiO_2 nanospheres.

2.3 Characterizations

The specific surface area and pore diameter of mSi and β-CD@mSi were measured using a V-sorb 2,800 analytical tester. The morphology and structure of mSi and β-CD@mSi were observed by a S-4800 (Hitachi, Japan) SEM. The

element distribution of β-CD@mSi was investigated using a Tecnai G2 F20 TEM (FEI, Hillsboro, OR, United States). Changes in elemental composition before and after β-CD@mSi adsorption were investigated using a ESCALAB 250 XI analyzer (Thermo, Waltham, MA, United States). IR was analyzed using a Nicolet 460 spectrometer (Thermo Fisher, Waltham, MA, United States).

2.4 Adsorption experiments

The effects of β-CD@mSi on RIF adsorption were studied by batch experiments under different conditions, including the amount of β-CD@mSi (10–50 mg), time (1–6 h), initial concentration of RIF (100–700 mg L^{-1}), pH (2–7), and temperature (288–308 K). Adjust the pH of the solution with 0.1 mol L^{-1} NaOH and HCl solution. A fixed amount of β-CD@mSi was added in 50.0 ml RIF solution. A series of adsorption experiments was carried out on a thermostatic oscillator (rotation frequency: 180 rpm). Residual RIF concentration was measured at the maximum absorbance (λ_{Max}) of 474 nm using an UV spectrophotometer (Hosseini et al., 2020). In order to guarantee the accuracy of experimental results, all test samples were tested in triplicate.

The adsorption capacity (qt) per Gram of β-CD@mSi and the removal efficiency of RIF at time t are calculated as follows: 1) The adsorption capacity of RIF; 2) Removal efficiency of RIF.

$$q_t = \frac{(C_0 - C_t)V}{M} \quad (1)$$

$$\text{RIF removal}(\%) = \frac{(C_0 - C_t)}{C_0} \times 100 \quad (2)$$

where C_0 is initial concentration (mg·L^{-1}); C_t is the concentration at completion of adsorption (mg·L^{-1}); V is the volume of RIF solution (L); M is the mass of adsorbent (g).

2.5 Quantum chemical calculation

Simulation calculations were performed using the Dmol3 module in Material Studio 2019. After structure optimization, then DNP 3.5 basis set was selected for calculation, and PBE of generalized gradient approximation (GGA) was selected for functional (Ghahghaey et al., 2020; Cao et al., 2021). In energy optimization, the SCF tolerance is 1.0×10^{-6}, the smearing is 0.005 Ha, water was used as solvent, and the dielectric constant is 78.54. According to density functional theory, HOMO, LUMO, and electrostatic potential were calculated (Tanzifi et al., 2020; Chen et al., 2021). The adsorption binding energy E_{ads} was calculated according to Eq. 3.

$$E_{ads} = E_{total} - E_{absorbate} - E_{adsorbent} \quad (3)$$

TABLE 1 Fitting results of adsorption kinetic model.

Kinetic models	Parameters	Temperature		
		288K	298K	308K
Pseudo first-order	q_e	99.69	106.81	123.37
	K_1	2.14	1.65	1.82
	R^2	0.99	0.991	0.998
Pseudo second-order	q_e	105.02	115.35	130.95
	K_2	0.05	0.02	0.03
	R^2	0.995	0.998	0.999
Elovich	R^2	0.952	0.955	0.994

where E_{total} is the Total energy, $E_{adsorbate}$ is the energy of rifampicin after optimization and $E_{adsorbent}$ is the energy of β-CD@mSi after optimization。

3 Results and analysis

3.1 Characterization of materials

3.1.1 SEM and BET analysis

The exterior morphology of mSi and β-CD@mSi were characterized by SEM, as shown in Figure 2A. The mSi has a smooth spherical shape and the diameter ranges from 100 to 150 nm. After loading with β-CD, the size of the composite material did not change significantly (Figure 2B). The N_2 adsorption and desorption isotherms of mSi and β-CD@mSi correspond to the type IV isotherm. The N_2 adsorption capacity of mSi and β-CD@mSi increases rapidly in the low pressure region, and remains relatively fixed in a wide pressure range with the increasing relative pressure, indicating that there are micropores and mesoporous pores in both mSi and β-CD@mSi. The BET surface area of mSi is 1,151.41 m^2/g, the total pore volume is 0.97 cm^3/g, and the average aperture size is 4.79 nm. After the β-CD is coated, the specific surface area of β-CD@mSi (418 m^2/g) and total pore volume (0.32 cm^3/g) decreased significantly. This indicates that β-CD enters the internal pore channels of the mesoporous silica nanospheres, thereby reducing the specific surface area and total pore volume (Neeli et al., 2018).

3.1.2 TEM analysis

In Supplementary Figure S3, TEM images of β-CD@mSi show that it is mainly composed of C, O, Si, and the distribution of C, O, and Si is uniform, indicating that β-CD@mSi is well prepared. The diameter of the monomeric particles of β-CD@mSi is around 150 nm, which is consistent with the SEM results. In addition, we also found that some C and O elements were distributed outside the blue spherical region of C and the green

TABLE 2 Fitting results of the isotherm model of β-CD@mSi.

Isothermal models	Parameters	Temperature (K)		
		288	298	308
Langmuir	q_{max}	254.78	273.32	388.15
	K_L	0.003	0.026	0.043
	R^2	0.416	0.709	0.78
	n	3.378	4.292	5.181
Freundlich				
	K_F	47.44	73.89	130.61
	R^2	0.913	0.98	0.993
Temkin	K_T	34.66	39.91	49.21
	f	7.89	1.45	0.05
	R^2	0.869	0.966	0.990

spherical region of O, indicating that β-CD was successfully loaded onto the surface of mSi.

3.1.3 XPS analysis

The element composition of β-CD@mSi surface before and after adsorption can be analyzed using XPS. The XPS spectra before and after adsorption of β-CD@mSi are shown in Supplementary Figure S4. The material has three elements, C, O and Si, which is consistent with the elemental composition of the material itself. Before adsorption, three peaks were fitted to the C1s spectrum at 284.8, 286.39 and 288.75 eV, corresponding to the C-C, C-O and O-C=O groups respectively (Zheng et al., 2018). Peaks fitted to the O1s spectrum at 532.41 eV and 533.27 eV correspond to C-O and C=O, which indicates that the composite The presence of oxygen-containing functional groups. The area corresponding to the C-C group and O=C-O group decreased and the area of the C-O group increased after adsorption. The peaks fitted to the O1s spectra at 532.41 eV and 533.27 eV shifted to 532.55 eV and 533.57 eV, corresponding to a decrease in the area of the C-O group and an increase in the area of the C=O group, which is related to the adsorption of rifampicin on the β-CD@mSi (Zhang et al., 2016). Following RIF adsorption, the N1s spectrum (Supplementary Figure S4D), showed a new fitted peak at 399.68 eV, which corresponded to the C-NH2 group on rifampicin, indicating that RIF had successfully adsorbed onto β-CD@mSi.

3.1.4 FTIR analysis

As shown in Supplementary Figure S5, the characteristic peaks of β-CD@mSi at 1,092, 1,635, 1700, and 3,440 cm^{-1} correspond to C-O, C-O-C, C-C, and O-H bonds of the composite materials, respectively. The appearance of the characteristic peaks of β-CD (C-O-C) indicates the successful loading of β-CD. The peak at 1,635 cm^{-1} represents the stretching vibration of the aromatic ring of β-CD. The infrared spectrum after adsorption has an obvious characteristic peak at 1,699 cm^{-1} and the intensity of the peak is obviously weakened, which corresponds to the stretching vibration of the amide bond on rifampicin, indicating that rifampicin was successfully adsorbed to β-CD@mSi (Yin et al., 2019).

3.2 Experimental influence parameter

3.2.1 Effect of adsorbent dosage

The removal rate of rifampicin increased with the increase of the dosage of β-CD@mSi, and the removal rate reached 90.95% at 0.8 g L^{-1}. As displayed in Supplementary Figure S6A, the results showed that with the increase of β-CD@mSi dose, the number of adsorption sites increased. The constant concentration of RIF solution leads to the decrease of adsorption capacity. Under the premise of ensuring the removal efficiency, 0.8 g L^{-1} was selected as the dosage.

3.2.2 Effect of pH

The removal efficiency of rifampicin was greatly affected by pH (Supplementary Figure S6B). The adsorption capacity of RIF decreased, when the pH gradually increased. According to zeta potential, when pH is between 1 and 6.1, rifampicin surface is still dominated by positive charge. When pH is between 6.1 and 7, the surface is dominated by negative charge. Since RIF has two pkas (1.7 and 7.9), when pH = 2, the ionization degree of RIF is the best, and removal of RIF is mainly through π–π interactions and hydrogen bonding. β-CD@mSi and RIF are electropositive, so the electrostatic attraction ability is very weak. It has been proved that intermolecular hydrogen bond strength decreases with the increase of pH (Rodriguez-Mozaz et al., 2015). With the increase of pH, the intermolecular hydrogen bonding is weakened, and the adsorption capacity decreases gradually. When pH = 7, both β-CD@mSi and RIF are electronegative, so the electrostatic attraction weakened and the adsorption capacity further decreased.

TABLE 3 Thermodynamic parameters.

Contaminant	ΔH_0 (kJ.mol^{-1})	ΔS_0 (kJ.mol^{-1})	ΔG_0 (kJ.mol^{-1})		
			288K	298K	308K
rifampicin	43.47	0.22	−9.24	−10.66	−12.48

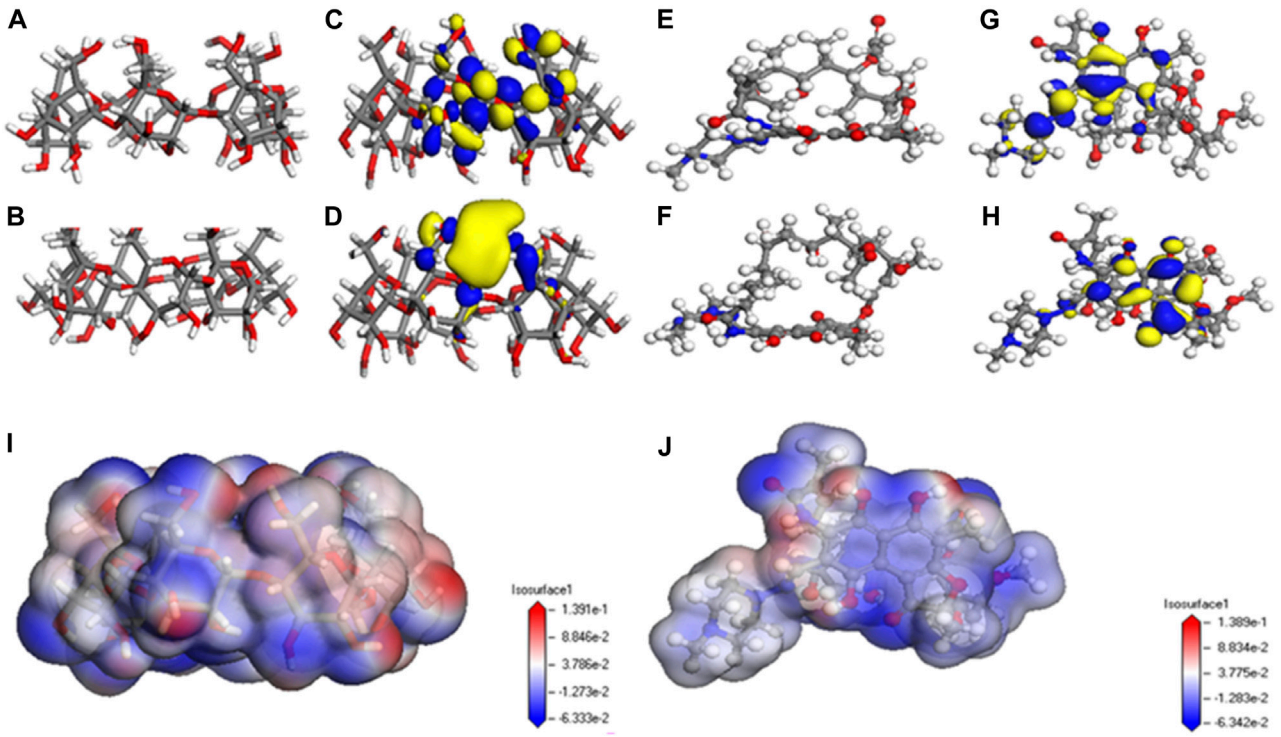

FIGURE 3
Simulation results of β-CD@mSi and rifampicin; **(A)** structure before optimization of β-CD@mSi; **(B)** the optimized structure of β-CD@mSi; **(C)** the highest occupied molecular orbital of β-CD; **(D)** the lowest unoccupied molecular orbital of RIF; **(E)** structure before optimization of RIF; **(F)** the optimized structure of RIF; **(G)** the highest occupied molecular orbital of RIF; **(H)** the lowest unoccupied molecular orbital of RIF; **(I)** surface electrostatic potential of β-CD; **(J)** surface electrostatic potential of RIF.

3.3 Adsorption kinetics

Pseudo-first-order model (Supplementary Equation S4), pseudo-second-order model (Supplementary Equation S5), Elovich model (Supplementary Equation S6), and Weber–Morris particle intra diffusion model (Supplementary Equation S7) were used to analyze the adsorption kinetics. The detailed calculation formula can be found in the supplementary literature.

The fitting results of β-CD@mSi are shown in Supplementary Figure S7. It can be found in Table 1 that the R^2 value of the quasi-second-order kinetic model is more in line with the experimental situation. Elovich model fitting results show that the adsorption process of RIF is chemisorption (Pandey et al., 2015). According to the intra-particle diffusion model, due to the large concentration difference between β-CD@mSi and RIF, we found the first line is steeper and can be thought to be the migration of RIF to the outer surface of β-CD@mSi by membrane diffusion. The second line is the intraparticle diffusion process. The third line shows adsorption equilibrium and its slope is relatively small. It is clear that the straight line in the first stage does not pass through the origin, membrane diffusion occurs simultaneously with intraparticle diffusion throughout the adsorption process (Wu et al., 2014; Asgharzadeha et al., 2019).

3.4 Adsorption isotherms

Description of adsorption isotherms by using the Langmuir model (Supplementary Equation S8), the Freundlich model (Supplementary Equation S9), and the Temkin model (Supplementary Equation S10). The detailed calculation formula can be found in the supplementary literature.

Supplementary Figure S8 is the fitting result of the adsorption isotherm model of β-CD@mSi. The theoretical adsorption capacity calculated by Langmuir is slightly different from the experimental result of RIF, and the fitting degree is poor. From the comparison of R^2 values (Table 2), it can be clearly seen that the Freundlich model is more in line with the process description, indicating that the adsorption of rifampicin by β-CD@mSi is a multilayer adsorption. Temkin isotherms describe the chemisorption of the adsorbent on the adsorbed material, confirming that the adsorption process is chemisorption.

10.3389/fchem.2022.1040435

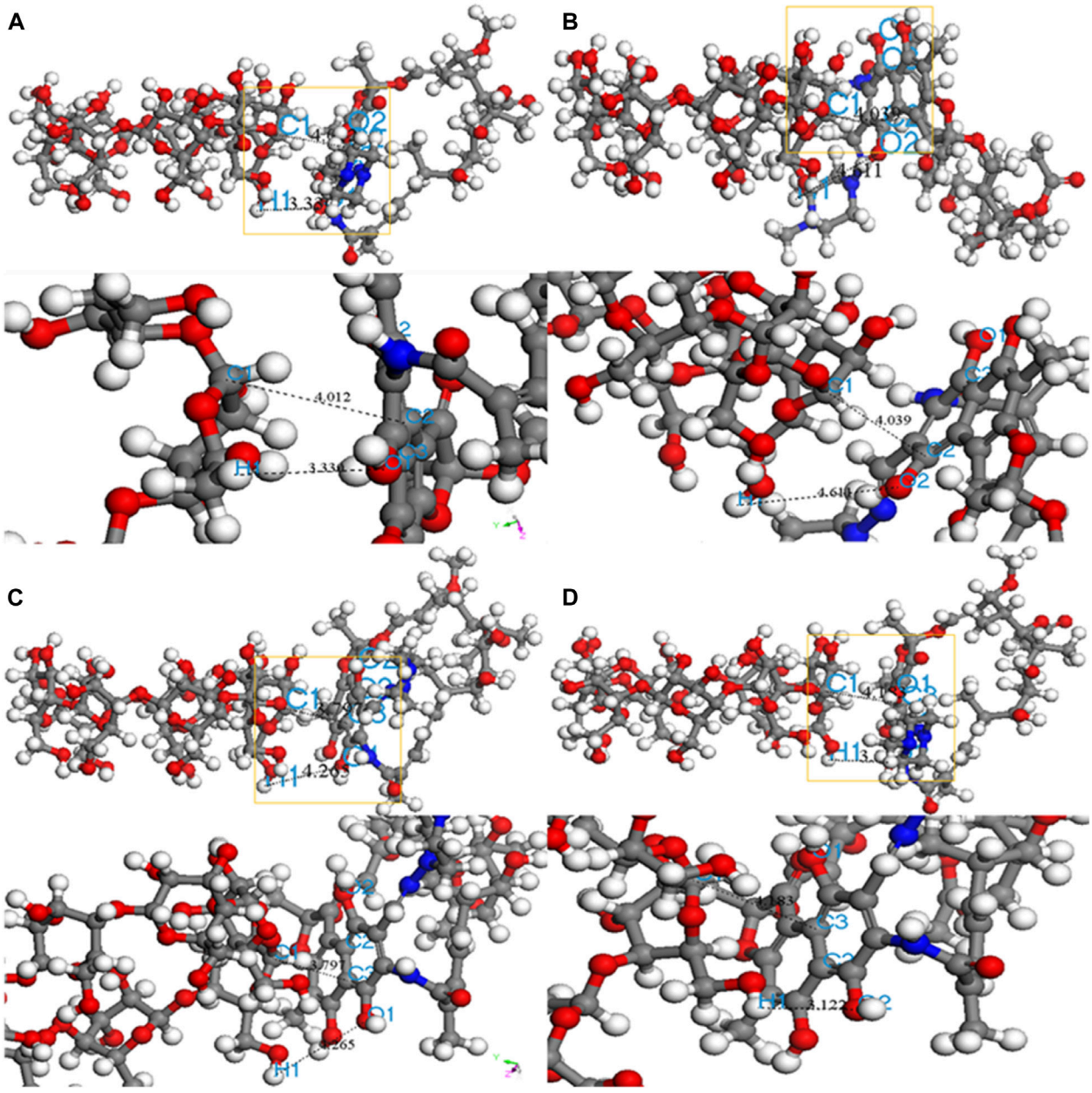

FIGURE 4
Four configurations of RIF aided on β -CD@mSi **(A)** C1-C2 H1-O1 adsorption configuration; **(B)** C1-C2 H1-O2 adsorption configuration; **(C)** C1-C3 H1-O1 adsorption configuration; **(D)** C1-C3 H1-O2 adsorption configuration.

TABLE 4 Binding energy results for the four corresponding structures.

Structure	Corresponding locus	Total energy (kcal/mol)	Binding energy (kcal/mol)
A	C1-C2;H1-O1	419.256	−17.660
B	C1-C2;H1-O2	418.667	−18.249
C	C1-C3;H1-O1	406.243	−30.673
D	C1-C3;H1-O2	422.769	−14.147

TABLE 5 Comparison of different adsorbents.

Adsorbent	Pollutants	Adsorption capacity ($mg.g^{-1}$)	Reference
Fe-NPs	Rifampicin	107.7	Lin et al. (2020)
Fe_3O_4	rifampicin	84.8	Cai et al. (2019)
rGO@Fe/Pd-NPs	rifampicin	90.9	Xu et al. (2020)
GO/CS/Fe_3O_4	rifampicin	101.22	Shafaati et al. (2020)
β-CD@mSi	rifampicin	246.75	This work

3.5 Adsorption thermodynamics

The detailed calculation formula of adsorption thermodynamics can be found in the supplementary literature. The Freundlich constant (K_F) is used to derive the equilibrium constant (Kc) (Tran et al., 2017), and the calculation results are shown in Table 3. As the temperature increases, the results for ΔG_0 are in the order -9.24, -10.66 and -12.48 kJ mol^{-1}. This indicates that RIF is more favorable at β-CD@mSi at high temperature, as the temperature rises, the adsorption effect of β-CD@mSi gets better. ΔH_0 = 43.47 kJ mol^{-1}. It indicates that the adsorption process is chemical adsorption (Tran et al., 2016). The adsorption of RIF at β-CD@mSi is a spontaneous endothermic process.

3.6 Removal mechanism of rifampicin by β-CD@mSi

Adsorption kinetics and isotherm results show that the adsorption of β-CD@mSi to RIF may be mainly chemisorption. According to the analysis of infrared spectroscopy and the results of XPS, we believe that the main adsorption mechanisms are π–π interaction between aromatic rings, intermolecular hydrogen bonding, and intermolecular electrostatic interaction. In order to explain the adsorption mechanism in more depth, we use the computer to simulate and calculate, and first optimize the structure of β-cyclodextrin and rifampicin (Safia et al., 2019; Liu et al., 2004). As shown in Figures 3B,F the cavity of the optimized rifampicin ring structure is obviously enlarged and the structure is more stable. According to density functional theory and frontier orbital theory, the HOMO and LUMO orbitals of β-cyclodextrin and rifampicin are calculated respectively, as shown in Figures 3C,D,G,H, the electron loss region of β-CD is mainly concentrated in the six-membered ring, and the electron gain region is concentrated in the hydroxymethyl group. The area where rifampicin gains and loses electrons is concentrated in the benzene ring and its adjacent aromatic ring. In contrast, the hydroxyl group on the ring is easier to get electrons. The electronegativity (χ) obtained from orbital calculations shows that the χ value of β-CD is −0.10041 Ha, and the χ value of RIF is −0.12475 Ha. Since electrons will flow from lower electronegativity to higher electronegativity, it indicates that the transfer direction of electrons is from β-CD to RIF. According to the previous judgment on the adsorption mechanism and the electron gain and loss area, we believe that the six-membered ring on β-CD interacts with the benzene ring on rifampicin. The hydrogen bonds are formed between the hydroxyl group on rifampicin and the C-H bond on β-CD. As shown in Figure 4, according to the surface electrostatic potential of β-CD and rifampicin, the surface potential of C atom near O atom on β-CD is positive, and we name this point C1. The surface potential of the benzene ring and the adjacent aromatic ring of rifampicin is negative, and the C atoms at the junction of the two rings are named C2 and C3, respectively. The surface potential of the hydroxymethyl group of β-CD is positive, and the H atom on the hydroxyl group is named H1. The surface potential of the hydroxyl groups on both sides of the benzene ring on rifampicin is negative, and the O atoms on the hydroxyl groups are named O1 and O2, respectively. We carried out the corresponding structure construction and simulation calculation, essentially adjusting the distance between hydrogen bonds and π–π. The calculation results are shown in Table 4. After calculation, structure C has the lowest binding energy, indicating that its overall structure is the most stable. We consider this structure to be the most stable configuration for rifampicin adsorption on β-CD@mSi (Chen et al., 2019; Yao et al., 2019; Chen et al., 2020). The distance between aromatic rings is 3.797 Å, and the π–π interaction was predominant in the reaction process. The intermolecular hydrogen bond distance of this configuration exceeds 3 Å, indicating the existence of weak hydrogen bonds between molecules. We therefore believe that π–π interaction was predominant in the reaction process, followed by intermolecular hydrogen bonding and electrostatic interactions (Hosseini et al., 2020).

3.7 Other adsorbents

As shown in Table 5, we compared β-CD@mSi with other rifampicin adsorption materials in the past 5 years, its adsorption

capacity has been greatly improved. In addition to the high specific surface area of β-CD@mSi, the abundant hydroxyl functional groups of β-CD provide more reactive sites for the adsorption of rifampicin, which enables β-CD@mSi to remove rifampicin not only through electrostatic attraction. This study shows that β-CD@mSi is a promising environmental material for antibiotic removal.

4 Conclusion

In this study, the *in situ* synthesis method was used to prepare β-CD@mSi, and the removal rate of rifampicin reached 90% in 298 K. The thermodynamic results show that the adsorption of rifampicin is a spontaneous endothermic chemical process. The results of adsorption isotherm show that RIF is multilayer adsorption on β-CD@mSi. Through computer simulation, The addition of β-CD enhances the π-π interaction between β-CD@mSi and RIF, thus enhancing the removal effect.π–π interaction is the dominant role in the adsorption process, followed by intermolecular hydrogen bonding and electrostatic attraction. Our research will contribute to the study of the preparation of environmental materials for RIF removal, β-CD@mSi has excellent environmental remediation properties and is suitable for future applications in wastewater treatment Bhattarai et al., 2014, Howes et al., 2007, Yin et al., 2019.

Data availability statement

The original contributions presented in the study are included in the article/Supplementary Material, further inquiries can be directed to the corresponding author.

Author contributions

XS and XK conceived and designed experiments. XS performed all experiments, statistical analysis and chemical analysis. JL assisted XS with his experiment. XS wrote manuscript. XK, YZ and JW guided the experiment, WL and MC provided technical assistance, XG, XRL and XL assisted in data processing, JW approved the main steps of the work. XG guided SX to analyze and explain the key data.

Funding

This research was supported by Liaoning Revitalization Talents Program [XLYC1807045].

Acknowledgments

This research was supported by Xingliao Talents Program [XLYC1807045]. Thanks for the research help from College of Energy and Environment, Shenyang Aerospace University and the College of Land and Environment, Shenyang Agricultural University.

Conflict of interest

The authors declare that the research was conducted in the absence of any commercial or financial relationships that could be construed as a potential conflict of interest.

Publisher's note

Supplementary material

The Supplementary Material for this article can be found online at: https://www.frontiersin.org/articles/10.3389/fchem.2022.1040435/full#supplementary-material

References

Asgharzadeha, F., Gholamib, M., Jonidib, A., Kermani, M., Asgharnia, H., and Rezaeikalantari, R. (2019). Study of tetracycline and metronidazole adsorption on biochar prepared from rice bran kinetics, isotherms and mechanisms. *Desalination Water Treat.* 159, 390–401. doi:10.5004/dwt.2019.24140

Bhattarai, B., Muruganandham, M., and Suri, R. P. (2014). Development of high efficiency silica coated β-cyclodextrin polymeric adsorbent for the removal of emerging contaminants of concern from water. *J. Hazard. Mat.* 273, 146–154. doi:10.1016/j.jhazmat.2014.03.044

Cai, W., Weng, X., and Chen, Z. (2019). Highly efficient removal of antibiotic rifampicin from aqueous solution using green synthesis of recyclable nano-Fe_3O_4. *Environ. Pollut.* 247, 839–846. doi:10.1016/j.envpol.2019.01.108

Cao, Y., Malekshah, R. E., Heidari, Z., Pelalak, R., Marjani, A., and Shirazian, S. (2021). Molecular dynamic simulations and quantum chemical calculations of adsorption process using amino-functionalized silica. *J. Mol. Liq.* 330, 115544. doi:10.1016/j.molliq.2021.115544

Chen, Q., Tang, Z., Li, H., Wu, M., Zhao, Q., and Pan, B. (2021). An electron-scale comparative study on the adsorption of six divalent heavy metal cations on MnFe2O4@CAC hybrid: Experimental and DFT investigations. *Chem. Eng. J.* 381, 122656. doi:10.1016/j.cej.2019.122656

Chen, Q., Wang, X., Yi, P., Zhang, P., Zhang, L., Wu, M., et al. (2020). Key roles of electron cloud density and configuration in the adsorption of sulfonamide antibiotics on carbonaceous materials: Molecular dynamics and quantum chemical investigations. *Appl. Surf. Sci.* 536, 147757. doi:10.1016/j.apsusc.2020.147757

Chen, Q., Zheng, J., Xu, J., Dang, Z., and Zhang, L. (2019). Insights into sulfamethazine adsorption interfacial interaction mechanism on mesoporous cellulose biochar: Coupling DFT/FOT simulations with experiments. *Chem. Eng. J.* 356, 341–349. doi:10.1016/j.cej.2018.09.055

Damasceno Junior, E., Almeida, J. M. F., Silva, I., do, N., Santos, L. M. d., Dias, E. F., et al. (2020). Obtaining and applying nanohybrid palygorskite-rifampicin in the pH-responsive release of the tuberculostatic drug. *Langmuir* 36 (34), 10251–10269. doi:10.1021/acs.langmuir.0c01834

de Sousa, S. M. R., Guimarães, L., Ferrari, J., De Almeida, W. B., and Nascimento, C. S. (2016). A DFT investigation on the host/guest inclusion process of prilocaine into β-cyclodextrin. *Chem. Phys. Lett.* 652, 123–129. doi:10.1016/j.cplett.2016.04.053

Degoutin, S., and BacquetNovel, M. (2012). Novel porous organosilica containing amino and β-cyclodextrin groups. *J. Porous Mat.* 20 (4), 663–671. doi:10.1007/s10934-012-9640-8

Ghahghaey, Z., Hekmati, M., and Ganji, M. D. (2020). Theoretical investigation of phenol adsorption on functionalized graphene using DFT calculations for effective removal of organic contaminants from wastewater. *J. Mol. Liq.* 324, 114777. doi:10.1016/j.molliq.2020.114777

Hosseini, H., and Mousavi, S. M. (2020). Density functional theory simulation for Cr(VI) removal from wastewater using bacterial cellulose/polyaniline. *Int. J. Biol. Macromol.* 165, 883–901. doi:10.1016/j.ijbiomac.2020.09.217

Howes, B. D., Guerrini, L., Sanchez-Cortes, S., Marzocchi, M. P., Garcia-Ramos, J. V., and Smulevich, G. (2007). The influence of pH and anions on the adsorption mechanism of rifampicin on silver colloids. *J. Raman Spectrosc.* 38, 859–864. doi:10.1002/jrs.1727

Kanakaraju, D., Glass, B. D., and Oelgemoeller, M. (2018). Advanced oxidation process-mediated removal of pharmaceuticals from water: A review. *J. Environ. Manage.* 219, 189–207. doi:10.1016/j.jenvman.2018.04.103

Khnifira, M., Boumya, W., Abdennouri, M., Sadiq, M., Achak, M., Serdaroglu, G., et al. (2021). A combined molecular dynamic simulation, DFT calculations, and experimental study of the eriochrome black T dye adsorption onto chitosan in aqueous solutions. *Int. J. Biol. Macromol.* 166, 707–721. doi:10.1016/j.ijbiomac.2020.10.228

Kuang, Y., Xia, Y., Wang, X., Rao, Q., and Yang, S. (2022). Magnetic surface molecularly imprinted polymer for selective adsorption of 4-hydroxycoumarin. *Front. Chem.* 10, 862777. doi:10.3389/fchem.2022.862777

Lin, Z., Weng, X., Owens, G., and Chen, Z. (2019). Simultaneous removal of Pb(II) and rifampicin from wastewater by iron nanoparticles synthesized by a tea extract. *J. Clean. Prod.* 242, 118476. doi:10.1016/j.jclepro.2019.118476

Liu, L., and Guo, Q. (2004). Use of quantum chemical methods to study cyclodextrin Chemistry. *J. Incl. Phenom. Macrocycl. Chem.* 50, 95–103. doi:10.1007/s10847-003-8847-3

Liu, Y., Johnson, N. W., Liu, C., Chen, R., Zhong, M., Dong, Y., et al. (2019). Mechanisms of 1, 4-dioxane biodegradation and adsorption by bio-zeolite in the presence of chlorinated solvents: Experimental and molecular dynamics simulation studies. *Environ. Sci. Technol.* 53, 14538–14547. doi:10.1021/acs.est.9b04154

Ma, L., Wang, Q., Islam, S. M., Liu, Y., Ma, S., and Kanatzidis, M. G. (2016). Highly selective and efficient removal of heavy metals by layered double hydroxide intercalated with the MoS_4^{2-} ion. *J. Am. Chem. Soc.* 138, 2858–2866. doi:10.1021/jacs.6b00110

Mallik, A. K., Moktadir, M. A., Rahman, M. A., and Shahruzzaman, M. (2022). Progress in surface-modified silicas for Cr(VI) adsorption: A review. *J. Hazard. Mater.* 423, 127041. doi:10.1016/j.jhazmat.2021.127041

Mao, S., Shen, T., Han, T., Ding, F., Zhao, Q., and Gao, M. (2021). Adsorption and co-adsorption of chlorophenols and Cr(VI) by functional organo-vermiculite: Experiment and theoretical calculation. *Sep. Purif. Technol.* 277, 119638. doi:10.1016/j.seppur.2021.119638

Marrane, S. E., Danoun, K., Allouss, D., Sair, S., Channab, B. E., Rhihil, A., et al. (2022). A novel approach to prepare cellulose-*g*-hydroxyapatite originated from natural sources as an efficient adsorbent for heavy metals: Batch Adsorption optimization via response surface methodology. *ACS omega* 7 (32), 28076–28092. doi:10.1021/acsomega.2c02108

Neeli, S. T., and Ramsurn, H. (2018). Synthesis and formation mechanism of iron nanoparticles in graphitized carbon matrices using biochar from biomass model compounds as a support. *Carbon* 134, 480–490. doi:10.1016/j.carbon.2018.03.079

Pandey, P., Sharma, S., and Sambi, S. (2015). Removal of lead(II) from waste water on zeolite-NaX. *J. Environ. Chem. Eng.* 3, 2604–2610. doi:10.1016/j.jece.2015.09.008

Rodriguez-Mozaz, S., Chamorro, S., Marti, E., Huerta, B., Gros, M., Sanchez-Melsio, A., et al. (2015). Occurrence of antibiotics and antibiotic resistance genes in hospital and urban wastewaters and their impact on the receiving river. *Water Res.* 69, 234–242. doi:10.1016/j.watres.2014.11.021

Safia, H., Ismahan, L., Abdelkrim, G., Mouna, C., Leila, N., and Fatiha, M. (2019). Density functional theories study of the interactions between host β-Cyclodextrin and guest 8-Anilinonaphthalene-1-sulfonate: Molecular structure, HOMO, LUMO, NBO, QTAIM and NMR analyses. *J. Mol. Liq.* 280, 218–229. doi:10.1016/j.molliq.2019.01.019

Shafaati, M., Miralinaghi, M., Shirazi, R. H. S. M., and Moniri, E. (2020). The use of chitosan/Fe_3O_4 grafted graphene oxide for effective adsorption of rifampicin from water samples. *Res. Chem. Intermed.* 46, 5231–5254. doi:10.1007/s11164-020-04259-9

Sikder, T., Rahman, M., Jakariya, Hosokawa, T., Kurasaki, M., and Saito, T. (2018). Remediation of water pollution with native cyclodextrins and modified cyclodextrins: A comparative overview and perspectives. *Chem. Eng. J.* 355, 920–941. doi:10.1016/j.cej.2018.08.218

Tanzifi, M., Yaraki, M. T., Beiramzadeh, Z., Heidarpoor Saremi, L., Najafifard, M., Moradi, H., et al. (2020). Carboxymethyl cellulose improved adsorption capacity of polypyrrole/CMC composite nanoparticles for removal of reactive dyes: Experimental optimization and DFT calculation. *Chemosphere* 255, 127052. doi:10.1016/j.chemosphere.2020.127052

Tian, B., Hua, S., Tian, Y., and Liu, J. (2020). Cyclodextrin-based adsorbents for the removal of pollutants from wastewater: A review. *Environ. Sci. Pollut. Res.* 28, 1317–1340. doi:10.1007/s11356-020-11168-2

Tran, H. N., You, S. J., and Chao, H. P. (2016). Thermodynamic parameters of cadmium adsorption onto orange peel calculated from various methods: A comparison study. *J. Environ. Chem. Eng.* 4 (3), 2671–2682. doi:10.1016/j.jece.2016.05.009

Tran, H. N., You, S. J., Hosseini-Bandegharaei, A., and Chao, H. P. (2017). Mistakes and inconsistencies regarding adsorption of contaminants from aqueous solutions: A critical review. *Water Res.* 120, 88–116. doi:10.1016/j.watres.2017.04.014

Wang, D., Jia, F., Wang, H., Chen, F., Fang, Y., Dong, W., et al. (2018). Simultaneously efficient adsorption and photocatalytic degradation of tetracycline by Fe-based MOFs. *J. Colloid Interface Sci.* 519, 273–284. doi:10.1016/j.jcis.2018.02.067

Wang, X., Li, F., Hu, X., and Hua, T. (2021). Electrochemical advanced oxidation processes coupled with membrane filtration for degrading antibiotic residues: A review on its potential applications, advances, and challenges. *Sci. Total Environ.* 784, 146912. doi:10.1016/j.scitotenv.2021.146912

Wei, J., Liu, Y., Li, J., Zhu, Y., Yu, H., and Peng, Y. (2019). Adsorption and co-adsorption of tetracycline and doxycycline by one-step synthesized iron loaded sludge biochar. *Chemosphere* 236, 124254. doi:10.1016/j.chemosphere.2019.06.224

Wu, Z., Zhong, H., Yuan, X., Wang, H., Wang, L., Chen, X., et al. (2014). Adsorptive removal of methylene blue by rhamnolipid-functionalized graphene oxide from wastewater. *Water Res.* 67, 330–344. doi:10.1016/j.watres.2014.09.026

Xiong, J. Q., Kurade, M., and Jeon, B. H. (2017). Biodegradation of levofloxacin by an acclimated freshwater microalga, Chlorella vulgaris. *Chem. Eng. J.* 313, 1251–1257. doi:10.1016/j.cej.2016.11.017

Xu, Q., Owens, G., and Chen, Z. (2020). Adsorption and catalytic reduction of rifampicin in wastewaters using hybrid rGO@ Fe/Pd nanoparticles. *J. Clean. Prod.* 264, 121617. doi:10.1016/j.jclepro.2020.121617

Yao, N., Li, C., Yu, J., Xu, Q., Wei, S., Tian, Z., et al. (2019). Insight into adsorption of combined antibiotic-heavy metal contaminants on graphene oxide in water. *Sep. Purif. Technol.* 236, 116278. doi:10.1016/j.seppur.2019.116278

Yin, Q., Liu, M., and Ren, H. (2019). Biochar produced from the co-pyrolysis of sewage sludge and walnut shell for ammonium and phosphate adsorption from water. *J. Environ. Manage.* 249, 109410. doi:10.1016/j.jenvman.2019.109410

Yin, W., Liu, L., Zhang, H., Tang, S., and Chi, R. (2019). A facile solvent-free and one- step route to prepare amino-phosphonic acid functionalized hollow mesoporous silica nanospheres for efficient Gd(III) removal. *J. Clean. Prod.* 243, 118688. doi:10.1016/j.jclepro.2019.118688

Zhang, C., Lai, C., Zeng, G., Huang, D., Yang, C., Wang, Y., et al. (2016). Efficacy of carbonaceous nanocomposites for sorbing ionizable antibiotic sulfamethazine from aqueous solution. *Water Res.* 95, 103–112. doi:10.1016/j.watres.2016.03.014

Zhang, Y., Jiang, F., Huang, D., Hou, S., Wang, H., Wang, M., et al. (2018). A facile route to magnetic mesoporous core–shell structured silicas containing covalently bound cyclodextrins for the removal of the antibiotic doxycycline from water. *RSC Adv.* 8, 31348–31357. doi:10.1039/c8ra05781h

Zhao, Z., Nie, T., and Zhou, W. (2019). Enhanced biochar stabilities and adsorption properties for tetracycline by synthesizing silica-composited biochar. *Environ. Pollut.* 254, 113015. doi:10.1016/j.envpol.2019.113015

Zheng, H., Gao, Y., Zhu, K., Wang, Q., Wakeel, M., Wahid, A., et al. (2018). Investigation of the adsorption mechanisms of Pb(II) and 1-naphthol by β-cyclodextrin modified graphene oxide nanosheets from aqueous solution. *J. Colloid Interface Sci.* 530, 154–162. doi:10.1016/j.jcis.2018.06.083